

RIS-Aided Integrated Sensing and Communication: Beamforming Designs and Antenna Selection

Yuying Mai^a, Mateen Ashraf^{cb}, Huiqin Du^{a,*} and Bo Tan^b

^aCollege of Information Science and Technology, Jinan University, 601 Huangpu Avenue West, 510632, Guangzhou, China

^bTampere Wireless Research Centre, Faculty of Information Technology and Communication Sciences, Tampere University, 33014 Tampere, Finland

ARTICLE INFO

Keywords:

Integrated sensing and communication
reconfigurable intelligent surface
beamforming design
antenna selection
energy efficiency

ABSTRACT

This work considers an integrated sensing and communication system, where a reconfigurable intelligent surface (RIS) is utilized to manage interference and radar signals. The sensors are attached to the RIS to sense multiple targets. A joint design of the base station transmit beamforming and RIS phase shift matrix is proposed to minimize total interference and maximize the worst received signal power at the RIS sensors. Due to highly coupled transmit beamforming and RIS phase matrices, the optimization problem is decoupled into two subproblems and solved iteratively by semidefinite programming and a manifold-based Riemannian steepest descent algorithm. We further design energy-aware beamforming to eliminate the interference induced by radar probing signals. Antenna selection with the ℓ_0 norm is introduced to exclude redundant antennas while maintaining the sufficient multiple beams for multiple users and targets with minimized required antennas. Due to the nonconvexity of the ℓ_0 -norm, we relax the number of active transmit antennas as a weighted ℓ_1 -norm and employ a concave approximation for the constraint on the radar beampattern. Numerical results illustrate that the proposed algorithms can effectively reduce interference and strengthen the received signal power for radar sensing, achieving mutual benefit for communication and sensing performance.

1. Introduction

Applications in the sixth generation (6G), including autonomous driving, smart city, and virtual reality, require significantly improved sensing and communication performance. Specifically, these applications demand ultra high data rates, ultra low latency, high energy efficiency and high reliability, and high precision/resolution sensing capabilities [1]. Integrated sensing and communication (ISAC) combines wireless communication functionality with sensing capability on a single platform, which can reduce hardware costs and overcome spectrum congestion issue.

The integrated functionality of sensing and communication can be achieved through waveform design and transmit beamforming. Initially, information-embedded transmit waveforms are designed to optimize radar capabilities under constraints of specific communication requirements. These optimizations include maximization of conditional mutual information (MI) between radar probing signal and echo [2][3], minimizing / maximizing beampattern mismatch / similarity [4–6], and minimization of Cramér-Rao bound (CRB) [7][8]. On the other hand, transmit beamforming designs are developed to maximize achievable sum rate [9][10], minimize multiuser interference (MUI) [11][12], maximize signal-to-interference-and-noise ratio (SINR) [13][14], while maintaining pre-specified constraints on radar

*Corresponding author

✉ yuyingmai@stu2021.jnu.edu.cn (Y. Mai); mateen.ashraf@tuni.fi (M. Ashraf); thuiqin.du@jnu.edu.cn (H. Du); bo.tan@tuni.fi (B. Tan)

performance. Recently, a trade-off between radar and communication has been explored in order to achieve mutual benefits for both functionalities [2, 15–19]. However, these designs were highly dependent on the number of signal streams. Even exploiting full multiple-input multiple-output (MIMO) degree-of-freedom (DoF), insufficient signal streams still result in rank deficiency of the covariance matrix for sensing multiple targets, leading to a singular Fisher information matrix (FIM) and an infeasible CRB [8, 17, 20]. To address this issue, the works of [5, 8, 21] employ extra probing streams dedicated to target probing without carrying the communication data that ensures full-rank covariance matrix and no distortion of MIMO radar sensing. All of the designs mentioned above work primarily on monostatic sensing, and the potential benefits of a bistatic ISAC system have not yet been investigated.

The reconfigurable intelligent surface (RIS) that can redirect incoming signals has been introduced as a means to minimize interference at communication terminals [12, 22–25]. It has recently been introduced into the ISAC system to improve communication and sensing performance. When adjusting the reflecting elements jointly with the dual functional radar communication waveform, RIS enhances the signal quality by minimizing MUI [23]. Mitigating MUI with the assistance of RIS is further investigated by optimizing the transmit waveform and the discrete phase shift under the CRB constraint [12]. In [25], RIS is used to reduce interference between uplink transmission and radar sensing in mobile edge computing. By optimizing its reflecting elements, the RIS effectively reinforces the desired signals while maintaining limited total energy consumption. Moreover, multiple RISs are deployed to mitigate interference between transmission and radar sensing on the transmitter and receiver, respectively [24]. By incorporating RISs, transmit beamforming facilitates efficient and reliable communication while minimizing interference to the radar system. The aforementioned studies highlight the potential of integrating RISs with ISAC to eliminate interference and improve both communication and sensing capabilities.

1.1. Related Work

Besides interference mitigation, a RIS is also utilized to enhance target sensing capabilities. The work in [26] introduces a self-sensing RIS architecture that relocates the direction of arrival (DoA) estimation of a target to dedicated sensors integrated at the RIS, rather than at the base station (BS). The omnidirectional RIS beampattern is generated to maximize the total power of the received signal at the sensors in the worst-case scenario. The work [27] further develops an atomic norm minimization-based algorithm which reduces the complexity of DoA estimation at RIS. Leveraging its capabilities of DoA estimation, RISs with dedicated sensors work as bistatic radar system for both communication and location sensing [28], which is different from conventional ISAC systems that BSs work as a monostatic radar [12, 23–25]. The work [19] further investigates the potential benefits of incorporating sensors with simultaneously transmitting and reflecting surfaces (STARS). By adjusting the RIS phase shift matrix, the received signals at the sensor are maximized while simultaneously reducing interference, thereby enhancing both sensing and

Table 1
System with RIS and Sensors

System	Optimization Problem	Loca. of RIS&Sensor	
		Seperated	Co-located
ISAC	Comm./Sensing	[32], [28]	[19], [29], [30], [31]
	Trade-off		our work
Sensing-only	DoA/CRB	[27]	[26]

communication performance. To address the challenges of multiplicative fading induced by multiple reflection, a sensing-RIS is introduced in an ISAC system to enhance the performance of CRB [29, 30], [31]. Furthermore, the impact of sensor location on radar sensing is investigated in [32], in which significant improvements can be achieved by incorporating sensors into an RIS. These valuable insights from advanced RIS applications and bistatic radar techniques inspire us to further investigate the implementation of sensors at RIS and the utilization of bistatic radar in the ISAC system. Moreover, Table 1 reveals that the trade-offs inherent in an ISAC system with a co-located sensor and RIS remain largely unaddressed.

Furthermore, energy and hardware efficiency are crucial considerations in ISAC systems, leading to a heightened focus on maximizing energy efficiency [33][34] and hybrid beamforming design [35]. In early 2004, antenna selection emerged as a low-cost low-complexity alternative to explore the benefits of MIMO systems [36, 37], and has recently been integrated into ISAC systems [17, 18, 38–41]. In [18], an antenna selection scheme is proposed to improve energy efficiency by activating the best subset of antennas using the $\ell_{1,\infty}$ -norm with better utilization of limited resources. Furthermore, advanced machine learning algorithms are utilized to accurately perform antenna selection [38, 39, 41] for selecting the optimal subset of the antenna to further improve the performance and efficiency of the MIMO radar with hybrid analog-digital beamforming [38]. All these designs strive to select the minimum activated antenna subset for energy efficiency and cost efficiency. However, minimizing only the activated antenna subset would cause the transmit covariance matrix to be rank-deficient, which would degrade the performance of MIMO radar, particularly in the transmit waveform design [20]. The trade-off between the energy efficiency of communication and the DoF for radar sensing has been largely overlooked.

1.2. Main Contributions

This work investigates a RIS-assisted bistatic ISAC system where sensors are located near the RIS. The BS transmits signals to multiple users while concurrently sensing targets with uncertain locations. The dual-functional operation inevitably leads to MUI and mutual interference between sensing and communication. The joint design of the transmit beamforming and RIS phase shifts is proposed to minimize total interference of the ISAC system while maximizing the minimum received signal power for radar sensing under various constraints, including the mismatch of the transmit beampattern, the transmit power, and the unit modulus constraint on the RIS phase shift. Simulation results validate

the importance of the minimum DoF provided by the covariance matrix of transmitted signals to sensing targets in the beamforming design. The proposed designs can reduce interference and strengthen the received signal power for sensing. Hardware cost and interference can be further reduced by energy-aware beamforming design with antenna selection. The contributions of this paper can be summarized as follows:

- We propose a RIS-assisted bistatic ISAC system, where sensors are positioned at the RIS to enhance radar sensing capabilities. Unlike conventional RIS-assisted ISAC systems, where the BS acts as a monostatic radar, this work introduces a configuration where the BS transmits radar probing signals while the sensors co-sited with RIS are deployed near the target area to receive signals for estimating the DoAs of potential targets. The developed configuration holds promise for reducing the severe product-distance round-trip path loss and provides less interference from the transmit array compared to a mono-static system, potentially enhancing the sensing accuracy. Since the beamforming designs in conventional RIS-assisted ISAC systems cannot be directly implemented, we develop optimum beamforming designs for the proposed RIS-assisted ISAC system.
- We develop a joint linear precoding design to ensure MIMO radar and communication performances. By combining linear precoded communication symbols and radar waveforms, the proposed approach generates a transmit signal with a rank-sufficient covariance matrix, facilitating accurate multiple-target sensing. Moreover, in contrast to conventional ISAC systems, RIS introduces an additional capability of enhancing the received power of reflected sensing signals at RIS sensors by adjusting its phase shifts. Therefore, the power of worst received radar signals and interference can be optimized.
- We develop an energy-aware beamforming that incorporates antenna selection to generate sufficient beams towards multiple targets while mitigating interference from radar probing signals. To ensure the minimum DoF for radar sensing, we determine the necessary number of activated antennas and investigate the relationship between the rank of the covariance matrix and the number of activated antennas. The proposed design reduces redundant transmit antennas by minimizing the ℓ_0 -norm of active beamforming, while ensuring that the number of activated antennas exceeds the minimum required rank of transmit covariance matrix for forming beampattern. The proposed design can reduce energy consumption of RF chains and achieve essential DoF for radar sensing without inducing radar interference at users.

1.3. Organization and Notations

The rest of this paper is organized as follows. Section 2 introduces the system model. Section 3 explores the joint transmit beamforming and passive beamforming design. Section 4 then proposes the energy-aware beamforming design with antenna selection. Simulation results are presented in Section 5, and the paper concludes with Section 6.

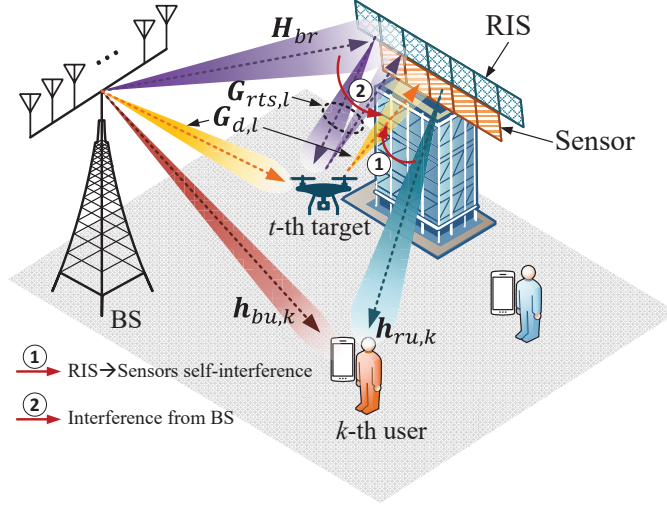


Figure 1: RIS-aided ISAC system.

Notations: Bold lower-case and upper-case letters denote column vectors and matrices, respectively. Normal font represents scalars. $(\cdot)^T$, $(\cdot)^*$, and $(\cdot)^H$ indicate the transpose, the complex conjugate, and the Hermitian transpose, respectively. \mathbb{R} and \mathbb{C} represent the set of real numbers and complex numbers, respectively. $\text{Re}(\cdot)$ denotes the real part of its argument. $\mathbb{E}(\cdot)$ stands for statistical expectation. $|a|$, $\|\mathbf{a}\|_0$, $\|\mathbf{a}\|_1$ and $\|\mathbf{A}\|_F$ denote the magnitude of a scalar a , the ℓ_0 norm and ℓ_1 norm of a vector \mathbf{a} , and the Forbenius norm of a matrix \mathbf{A} . \odot stands for the Hadamard product. $\text{tr}(\cdot)$ takes the trace of the argument. $\mathcal{CN}(\mathbf{0}, \mathbf{\Sigma})$ designates the Gaussian distribution with mean $\mathbf{0}$ and covariance matrix $\mathbf{\Sigma}$. $\text{diag}(\cdot)$, $\text{blkdiag}(\cdot)$ and $\text{vec}(\cdot)$ denote diagonalization, block diagonalization and vectorization, respectively. $\delta(\cdot)$ is the delta function with respect to the argument. $\text{rank}(\cdot)$ denotes the rank of the argument.

2. System Model

This work considers a RIS-aided ISAC system that senses radar targets and serves downlink users simultaneously. As shown in Fig.1, BS equipped with N_t transmit uniform linear array (ULA) antennas communicate with K single-antenna users while sensing T point targets. The targets are assumed to be located within distinct target areas, with their specific positions unknown. To enhance sensing capabilities and mitigate mutual interference between radar and communication, an ULA-based RIS, equipped with N_r passive reflecting elements, is deployed close to the areas of interest where targets and users are located. Different from previous RIS-assisted works where the BS performs the sensing function by processing the echo signals which have experienced multi-hop reflections and multiplicative fading, this work follows the configuration of [26] that deploys the sensors at RIS. This configuration avoids the high path-loss effects during the complex propagation. Meanwhile, the sensors on the RIS would have more stable and improved sensing signals, which can enhance detection and estimation performance. According to the configuration, sensors N_s are installed adjacent to the RIS elements, which can receive the signals from the targets and passively sense the targets

[32] [42]. Due to co-location fact of sensors and RIS, when the echo signal from the target is arriving at sensors, it will be interfered by two interfering signals: **i)** BS→RIS signal; **ii)** RIS→user signal. These unwanted interfering signals can be eliminated by the generalized sidelobe canceller [43] or background channel estimation [26]. These unintended signals can be eliminated by advanced techniques. For simplicity, we focus on the target angle estimation based on the received signals at the RIS sensors in this paper. Moreover, in this study, we assume the availability of perfect channel state information (CSI) and synchronization, concentrating our efforts on the effectiveness of beamforming design to optimize the trade-offs inherent in the bistatic RIS-assisted ISAC system. The scope of our research currently excludes scenarios with imperfections at this stage.

2.1. Communication Model

In this system, the BS transmits the communication symbols and radar probing signals concurrently. The transmitted signals $\mathbf{X} \in \mathbb{C}^{N_t \times M}$ from BS are the weighted sum of communication symbols and dedicated radar probing signals [5][21], that is

$$\mathbf{X} = \mathbf{W}\mathbf{S} = \mathbf{W}_c\mathbf{S}_c + \mathbf{W}_r\mathbf{S}_r, \quad (1)$$

where $\mathbf{W} = [\mathbf{W}_c, \mathbf{W}_r] \in \mathbb{C}^{N_t \times (K+N_t)}$, $\mathbf{S} = [\mathbf{S}_c; \mathbf{S}_r] \in \mathbb{C}^{(K+N_t) \times M}$, the matrix $\mathbf{W}_c = [\mathbf{w}_1, \dots, \mathbf{w}_K] \in \mathbb{C}^{N_t \times K}$ denotes the communication precoder, and $\mathbf{S}_c = [\mathbf{s}_1^c, \dots, \mathbf{s}_M^c] \in \mathbb{C}^{K \times M}$ represents the transmitted communication symbols with M length of blocks. Similarly, $\mathbf{W}_r = [\mathbf{w}_1, \dots, \mathbf{w}_{N_t}] \in \mathbb{C}^{N_t \times N_t}$ denotes the precoder for the radar probing signal $\mathbf{S}_r = [\mathbf{s}_1^r, \dots, \mathbf{s}_M^r] \in \mathbb{C}^{N_t \times M}$. Besides, $\text{tr}(\mathbf{W}\mathbf{W}^H) = P_t$, and P_t is the transmit power. Without loss of generality, it is assumed that $\mathbb{E}[\mathbf{s}_m^c(\mathbf{s}_m^c)^H] = \mathbf{I}_{K \times K}$, $\mathbb{E}[\mathbf{s}_m^r(\mathbf{s}_m^r)^H] = \mathbf{I}_{N_t \times N_t}$, and $\mathbb{E}[\mathbf{s}_m^c(\mathbf{s}_m^r)^H] = \mathbf{0}_{K \times N_t}$. The covariance matrix $\mathbf{R} \in \mathbb{C}^{N_t \times N_t}$ of the transmitted signals can be given by

$$\mathbf{R} = \mathbb{E}(\mathbf{X}\mathbf{X}^H) = \mathbf{W}_c\mathbf{W}_c^H + \mathbf{W}_r\mathbf{W}_r^H. \quad (2)$$

With the aid of the RIS, the users receive signals transmitted by the BS through the direct link and the RIS-reflected link. Let $\mathbf{H}_{br} \in \mathbb{C}^{N_t \times N_t}$ denote the channel from the BS to the RIS, it can be modelled as

$$\mathbf{H}_{br} = \sqrt{\frac{K_R}{1+K_R}}\mathbf{H}_{LOS} + \sqrt{\frac{1}{1+K_R}}\mathbf{H}_{NLOS}, \quad (3)$$

where K_R is the Rician factor, \mathbf{H}_{LOS} is the line-of-sight (LOS) deterministic component and \mathbf{H}_{NLOS} denotes the non-LOS (NLOS) Rayleigh fading component. Let $\mathbf{H}_{bu} = [\mathbf{h}_{bu,1}, \dots, \mathbf{h}_{bu,K}]^T \in \mathbb{C}^{K \times N_t}$ be the downlink channels between the BS and the users, which follow the Rayleigh distribution, and it can be presented as $\mathbf{h}_{bu,k} = \sqrt{\bar{\alpha}_k}\bar{\mathbf{h}}_{bu,k}$, where $\bar{\alpha}_k$ contains the path loss of BS to the user k and the shadow fading coefficients, and $\bar{\mathbf{h}}_{bu,k} \sim \mathcal{CN}(\mathbf{0}, \mathbf{I}_{N_t})$. The

channels between the RIS and users are represented as the matrix $\mathbf{H}_{ru} = [\mathbf{h}_{ru,1}, \dots, \mathbf{h}_{ru,K}]^T \in \mathbb{C}^{K \times N_I}$, whose column vectors can be similarly defined as $\mathbf{h}_{ru,k} = \tilde{\alpha}_k^{1/2} \tilde{\mathbf{h}}_{ru,k}$ with the path loss $\tilde{\alpha}_k$ and $\tilde{\mathbf{h}}_{ru,k} \sim \mathcal{CN}(\mathbf{0}, \mathbf{I}_{N_I})$.

The received signals $\mathbf{Y} \in \mathbb{C}^{K \times M}$ at the downlink users through two links can be given by [12, 15, 44]

$$\begin{aligned} \mathbf{Y} &= (\mathbf{H}_{bu} + \mathbf{H}_{ru} \mathbf{\Theta} \mathbf{H}_{br}) \mathbf{X} + \mathbf{N}_0 \\ &= \tilde{\mathbf{H}}_{bu} \mathbf{W}_c \mathbf{S}_c + \tilde{\mathbf{H}}_{bu} \mathbf{W}_r \mathbf{S}_r + \mathbf{N}_0 \\ &= \underbrace{(\tilde{\mathbf{H}}_{bu} \mathbf{W}_c \mathbf{S}_c - \bar{\mathbf{S}}_c)}_{\text{MUI}} + \underbrace{\tilde{\mathbf{H}}_{bu} \mathbf{W}_r \mathbf{S}_r}_{\text{radar interference}} + \bar{\mathbf{S}}_c + \mathbf{N}_0, \end{aligned} \quad (4)$$

where the phase shift matrix of RIS $\mathbf{\Theta} = \text{diag}(\boldsymbol{\theta})$ is defined by reflection vector $\boldsymbol{\theta} = [e^{i\theta_1}, \dots, e^{i\theta_{N_I}}]^T$ with unit modulus $|\theta_n| = 1, \forall n = 1, \dots, N_I$, $\tilde{\mathbf{H}}_{bu} = (\mathbf{H}_{bu} + \mathbf{H}_{ru} \mathbf{\Theta} \mathbf{H}_{br})$, and $\mathbf{N}_0 = [\mathbf{n}_1, \dots, \mathbf{n}_K]^T \in \mathbb{C}^{K \times M}$ is the zero-mean white Gaussian noise (AWGN) matrix with $\mathbf{n}_k \sim \mathcal{CN}(\mathbf{0}, \sigma^2 \mathbf{I})$, $\forall k = 1, \dots, K$. The desired constellation symbol matrix is defined as $\bar{\mathbf{S}}_c = \sqrt{P_t} \mathbf{S}_c = [\bar{\mathbf{s}}_1, \dots, \bar{\mathbf{s}}_M]$. Note that the aforementioned channels are under quasi-static block flat fading [20].

In an ISAC system, without cooperation among users or prior information on the received radar probing signal, simultaneous communication and radar sensing result in not only MUI but also radar interference, leading to severe degradation of system performance [45]. The total interference can be measured as the sum of MUI and radar interference, that is,

$$\begin{aligned} P_{intf} &= \left\| \tilde{\mathbf{H}}_{bu} \mathbf{W}_c \mathbf{S}_c - \bar{\mathbf{S}}_c \right\|_F^2 + \left\| \tilde{\mathbf{H}}_{bu} \mathbf{W}_r \mathbf{S}_r \right\|_F^2 \\ &= \left\| \tilde{\mathbf{H}}_{bu} \mathbf{W} \mathbf{S}_1 - \mathbf{S}_2 \right\|_F^2, \end{aligned} \quad (5)$$

where $\mathbf{S}_2 = [\bar{\mathbf{S}}_c, \mathbf{0}]$ and $\mathbf{S}_1 = \text{blkdiag}(\mathbf{S}_c, \mathbf{S}_r) \in \mathbb{C}^{(K+N_I) \times 2M}$. It should be noted that, as demonstrated in Eq.(4) [15], the SINR of the communication users is a monotonically decreasing function of MUI, assuming that the signal power and the system noise level remain constant. Therefore, minimizing MUI is equivalent to maximizing SINR, and in turn leads to the enhancement of the achievable sum rate [15, 23].

2.2. Radar Model

From the sensing perspective, the system can be viewed as a bistatic radar configuration wherein the BS transmits the probing signals and the sensor at RIS captures the reflected signals from targets.

In practice, the distance can be estimated by measuring the round-trip time [46], but the exact locations of the targets are unknown, with only the possible regions based on prior knowledge [47][48], such as the unmanned aerial vehicle localization scenario. Specifically, the T targets are assumed to be located in T distinguish subareas, each with

Q possible angles. The total possible angles $\boldsymbol{\phi} \in \mathbb{C}^{L \times 1}$ of all targets are denoted as

$$\boldsymbol{\phi} = \underbrace{[\phi_1, \dots, \phi_Q, \dots]}_{1\text{-st subarea}}, \underbrace{[\phi_{(t-1)Q+1}, \dots, \phi_{tQ}, \dots]}_{t\text{-th subarea}}, \underbrace{[\phi_{(T-1)Q+1}, \dots, \phi_{TQ}]}_{T\text{-th subarea}}^T, \quad (6)$$

where $L = T \times Q$ and the l -th element $\phi_l, l \in \mathcal{L} \triangleq \{1, \dots, L\}$, is defined as the possible angle l of target.

The sensors at RIS receive signals reflected by possible target t through two distinct links. One is from the BS to the potential target t and then to the sensors at the RIS, that is, BS \rightarrow target \rightarrow RIS sensors, represented by the channel matrix $\mathbf{G}_{d,l} \in \mathbb{C}^{N_s \times N_t}$. The other involves transmission from the BS to the RIS elements, reflection to the potential target t , and finally reception at the sensors near the RIS, that is, BS \rightarrow RIS elements \rightarrow target \rightarrow sensors at RIS, which is denoted by the channel matrix $\mathbf{G}_{r,l} \in \mathbb{C}^{N_s \times N_t}$. It is important to note that the channels between BS/RIS and UAV targets are ground-to-air links. It can be treated as a clutter-free environment [49][50].

Suppose the steering vector of an N -element ULA towards direction φ is given by $\mathbf{a}(\varphi, N)$. The RIS-reflected link $\mathbf{G}_{r,l}$ can be defined as

$$\mathbf{G}_{r,l} = \mathbf{G}_{rts,l} \boldsymbol{\Theta} \mathbf{H}_{br} = \rho_{lr} \beta_l \mathbf{a}(\varphi_l, N_s) \mathbf{a}^H(\varphi_l, N_t) \boldsymbol{\Theta} \mathbf{H}_{br}, \quad (7)$$

where ρ_{lr} and β_l are the complex path loss from RIS elements to sensors via possible target t and the reflectivity of possible target t , respectively. The link $\mathbf{G}_{rts,l}$ is clutter-free channel and can be defined as the path RIS elements \rightarrow target \rightarrow sensors at RIS. The angle of arrival (AoA) φ_l from the possible angle l of target t to the sensors at RIS can be considered identical to the angle of the RIS elements to the target t under the condition of the far field. The direct link associated with the potential target t is denoted by $\mathbf{G}_{d,l} \in \mathbb{C}^{N_s \times N_t}$, that is,

$$\mathbf{G}_{d,l} = \rho_{ld} \beta_l \mathbf{a}(\varphi_l, N_s) \mathbf{a}^H(\varphi_l, N_t), \quad (8)$$

where ρ_{ld} is the complex path loss from BS to sensors via possible target t .

The superimposed signals received at the sensors from the potential target t can be given by

$$\mathbf{Y}_{s,l} = (\mathbf{G}_{d,l} + \mathbf{G}_{r,l}) \mathbf{W} \mathbf{S}_1 + \mathbf{N}_s, \quad (9)$$

where $\mathbf{N}_s = [\mathbf{n}_1, \dots, \mathbf{n}_{N_s}]^T \in \mathbb{C}^{N_s \times M}$ is the noise matrix at the sensors with $\mathbf{n}_s \sim \mathcal{CN}(\mathbf{0}, \sigma_s^2 \mathbf{I})$. Note that, in the clutter-free environment, there is no signal-dependent interference typically associated with ground-based reflections.

Hence, the received signals power at the sensors co-sited with RIS from the potential target t can be given by

$$\begin{aligned} P_l &= \left\| (\mathbf{G}_{d,l} + \mathbf{G}_{r,l}) \mathbf{W} \mathbf{S}_1 \right\|_F^2 \\ &= \text{tr}((\mathbf{G}_{d,l} + \mathbf{G}_{r,l}) \mathbf{W} \mathbf{W}^H (\mathbf{G}_{d,l} + \mathbf{G}_{r,l})^H), \end{aligned} \quad (10)$$

where $\mathbf{S}_1 \mathbf{S}_1^H = \mathbf{I}_{K+N_t}$. In the absence of precise target locations, maximizing the worst-case received signal power at sensors can enhance the sensing capabilities.

To sense potential targets, the transmitted beampattern points to the target area by designing the beamforming matrix. The transmit beampattern in the direction ϕ_d is

$$P(\phi_d, \mathbf{W}) = \mathbf{a}^H(\phi_d) \mathbf{W} \mathbf{W}^H \mathbf{a}(\phi_d), \quad (11)$$

where $\mathbf{a}(\phi_d)$ is the transmit steering vector of direction ϕ_d . The beampattern similarity can be measured by calculating the mean square error (MSE) between the desired beampattern and the obtained beampattern [6], that is,

$$L_r(\mathbf{W}, \lambda) = \frac{1}{D} \sum_{d=1}^D \left| \lambda d(\phi_d) - P(\phi_d, \mathbf{W}) \right|^2, \quad (12)$$

where λ is a scaling factor restricted by the transmit power, $d(\phi)$ is the desired beampattern, and $\{\phi_d\}_{d=1}^D$ are sampled angles with D discrete grids covering the location sectors of interest (i.e., target area).

3. Joint Transmit Beamforming and Passive Beamforming Design

With the constraints of the radar and RIS phase shift, we design the transmit beamforming and passive beamforming for both radar and communication and then reformulate the optimization problem into a tractable problem.

3.1. Problem Formulation

In this work, we design the transmit beamforming and RIS phase shift matrix to balance communication and radar performance. Focusing on unit consistency, we utilize power as the unified metric. The objective is to minimize the interference power for enhancing communication quality while maximizing the worst received signal power at sensors to maintain sensing capabilities, that is,

$$\min_{\mathbf{W}, \Theta, \lambda} \frac{\rho}{Q_c} \left\| \tilde{\mathbf{H}}_{bu} \mathbf{W} \mathbf{S}_1 - \mathbf{S}_2 \right\|_F^2 + \frac{1-\rho}{Q_s} \left(-\min_l P_l \right) \quad (13a)$$

$$\text{s.t.} \quad \frac{1}{D} \sum_{d=1}^D \left| \lambda d(\phi_d) - \mathbf{a}^H(\phi_d) \mathbf{W} \mathbf{W}^H \mathbf{a}(\phi_d) \right|^2 \leq \epsilon_p, \quad (13b)$$

$$\text{tr}(\mathbf{W}\mathbf{W}^H) = P_t, \quad (13c)$$

$$|\theta_n| = 1, \quad \forall n = 1, \dots, N_I, \quad (13d)$$

where Q_c and Q_s are empirically determined, balancing the total interference and the received signal power, and $\rho \in (0, 1)$ is the weighting factor determining the trade-off between radar and communication performance. The underlying problem involves a multiple-objective optimization task focused on reducing interference power and augmenting the received signal power at sensors co-sited with RIS. Moreover, since one of the sensing signals reaching the target is from BS to target via RIS, optimizing the RIS phase shift matrix can further enhance the signal power at target, and consequently, amplify the received signal power at sensor. Constraint (13b) guarantees that the MSE of the beampattern is less than the threshold ε_p . (13c) represents the transmit power budget constraint. The constraint (13d) denotes the unit-modulus constraint of the RIS phase shift.

Remark 1: In ISAC systems, it is common to optimize the multi-objective optimization problem across various scales and units [15, 16, 51]. However, our approach guarantees unit consistency by adopting power as a unified metric, with a focus on minimizing interference power for communication and maximizing the worst case received signal power at sensors for sensing.

Furthermore, the constraint (13b) from (12) is a convex quadratic function w.r.t the variable λ . The optimal λ can be obtained by taking the derivative of (13b) with respect to λ and setting it equal to 0 [4], that is,

$$\frac{1}{D} \sum_{d=1}^D [2\lambda d^2(\phi_d) - 2d(\phi_d)\mathbf{a}^H(\phi_d)\mathbf{W}\mathbf{W}^H\mathbf{a}(\phi_d)] = 0, \quad (14)$$

$$\lambda^* = \frac{1}{\sum_{d=1}^D d^2(\phi_d)} \sum_{d=1}^D d(\phi_d) \text{vec}(\mathbf{A}_d) \text{vec}(\mathbf{W}\mathbf{W}^H), \quad (15)$$

where $\text{vec}(\mathbf{A}_d)\text{vec}(\mathbf{W}\mathbf{W}^H) = \mathbf{a}^H(\phi_d)\mathbf{W}\mathbf{W}^H\mathbf{a}(\phi_d)$ and $\mathbf{A}_d \triangleq \mathbf{a}(\phi_d)\mathbf{a}^H(\phi_d)$ for brevity. Substituting (15) into (12), the MSE of the beampattern $L_r(\mathbf{W}, \lambda)$ is reduced to

$$L_r(\mathbf{W}) = \sum_{d=1}^D \left| \mathbf{d}_d^H \text{vec}(\mathbf{W}\mathbf{W}^H) \right|^2, \quad (16)$$

where $\mathbf{d}_d^H \triangleq \frac{1}{\sqrt{D} \sum_{d=1}^D d^2(\phi_d)} d(\phi_d) \sum_{d=1}^D d(\phi_d) \text{vec}^H(\mathbf{A}_d) - \frac{1}{\sqrt{D}} \text{vec}^H(\mathbf{A}_d)$.

Since the variable λ is only related to the constraint (13b), the optimization problem (13) is reformulated as

$$\min_{\mathbf{W}, \Theta} \frac{\rho}{Q_c} \left\| \tilde{\mathbf{H}}_{bu} \mathbf{W} \mathbf{S}_1 - \mathbf{S}_2 \right\|_F^2 + \frac{1-\rho}{Q_s} \left(-\min_l P_l \right) \quad (17a)$$

$$s.t. \sum_{d=1}^D \left| \mathbf{d}_d^H \text{vec}(\mathbf{W} \mathbf{W}^H) \right|^2 \leq \varepsilon_p, \quad (17b)$$

$$(13c), (13d).$$

However, the variables \mathbf{W} and Θ are highly coupled in (17a) and all constraints, which makes the problem (17) quite challenging. To address this problem, \mathbf{W} and Θ can be optimized via an alternating optimization algorithm.

3.2. Optimization of \mathbf{W} with Given Θ

With given Θ , the problem (17) with respect to \mathbf{W} can be recast as follows,

$$\min_{\mathbf{W}, t} \frac{\rho}{Q_c} I(\mathbf{W}) + \frac{1-\rho}{Q_s} (-t) \quad (18a)$$

$$s.t. \text{tr} \left((\mathbf{G}_{d,l} + \mathbf{G}_{r,l}) \mathbf{W} \mathbf{W}^H (\mathbf{G}_{d,l} + \mathbf{G}_{r,l})^H \right) \geq t, \forall l, \quad (18b)$$

$$(17b), (13c),$$

where t is the introduced auxiliary variable and $I(\mathbf{W}) = \text{tr}(\mathbf{W} \mathbf{W}^H \mathbf{B}_1) - 2\text{Re} \left(\text{tr} \left(\tilde{\mathbf{H}}_{bu} \mathbf{W} \mathbf{D}_1^H \right) \right)$ with $\mathbf{B}_1 = \tilde{\mathbf{H}}_{bu}^H \tilde{\mathbf{H}}_{bu}$ and $\mathbf{D}_1 = \mathbf{S}_2 \mathbf{S}_1^H = [P_l \mathbf{I}_{K \times K}, \mathbf{0}_{K \times N_l}]$.

However, the underlying problem is a nonconvex quadratically constrained quadratic programming (QCQP) problem, generally NP-hard. To address this issue, the SDP approach can be applied by relaxing (2) as a positive semi-definiteness constraint $\mathbf{R} - \mathbf{W} \mathbf{W}^H \geq \mathbf{0}$. By applying the Schur complement [52], the subproblem (18) can be written as

$$\min_{\mathbf{W}, \mathbf{R}, t} \frac{\rho}{Q_c} I(\mathbf{W}, \mathbf{R}) + \frac{1-\rho}{Q_s} (-t) \quad (19a)$$

$$s.t. \sum_{d=1}^D \left| \mathbf{d}_d^H \text{vec}(\mathbf{R}) \right|^2 \leq \varepsilon_p, \text{tr}(\mathbf{R}) = P_t, \quad (19b)$$

$$\text{tr} \left((\mathbf{G}_{d,l} + \mathbf{G}_{r,l}) \mathbf{R} (\mathbf{G}_{d,l} + \mathbf{G}_{r,l})^H \right) \geq t, \forall l, \quad (19c)$$

$$\begin{bmatrix} \mathbf{R} & \mathbf{W} \\ \mathbf{W}^H & \mathbf{I} \end{bmatrix} \geq \mathbf{0}. \quad (19d)$$

Now, it can be efficiently solved in polynomial time by using off-the-shelf solvers such as the CVX toolbox.

3.3. Optimization of Θ with Given \mathbf{W}

By defining $\theta = \text{diag}(\Theta)$, the interference (5) is recast as

$$I(\theta) = \theta^H (\mathbf{B}_2 \odot \mathbf{C}_1^T) \theta + 2\text{Re}(\tilde{\mathbf{a}}^T \theta - \theta^H \mathbf{d}_2), \quad (20)$$

where $\mathbf{B}_2 = \mathbf{H}_{ru}^H \mathbf{H}_{ru}$, $\mathbf{C}_1 = \mathbf{H}_{br} \mathbf{W} \mathbf{W}^H \mathbf{H}_{br}^H$, $\tilde{\mathbf{a}} = \text{diag}(\mathbf{H}_{br} \mathbf{W} \mathbf{W}^H \mathbf{H}_{bu}^H \mathbf{H}_{ru})$ and $\mathbf{d}_2 = \text{diag}(\mathbf{H}_{ru}^H \mathbf{D}_1 \mathbf{W}^H \mathbf{H}_{br}^H)$.

The minimum received signal power P_{l^\dagger} at the sensors of the potential target t^\dagger can be found by searching $\{P_l\}_{l=1}^L$. According to the formulation of P_{l^\dagger} , after omitting the terms not related to Θ , $P_{l^\dagger}(\Theta)$ is recast as

$$S^\dagger(\theta) = \theta^H (\mathbf{B}_3 \odot \mathbf{C}_1^T) \theta + \mathbf{c}_2^T \theta + \theta^H \mathbf{c}_2^*, \quad (21)$$

where $\mathbf{c}_2 = \text{diag}(\mathbf{H}_{br} \mathbf{W} \mathbf{W}^H \mathbf{G}_{d,l^\dagger}^H \mathbf{G}_{rts,l^\dagger})$, $\mathbf{B}_3 = \mathbf{G}_{rts,l^\dagger}^H \mathbf{G}_{rts,l^\dagger}$ with $\mathbf{G}_{rts,l^\dagger} = \rho_{l^\dagger r} \beta_{l^\dagger} \mathbf{a}(\varphi_{l^\dagger}, N_S) \mathbf{a}^H(\varphi_{l^\dagger}, N_I)$ and $\mathbf{G}_{d,l^\dagger} = \rho_{l^\dagger d} \beta_{l^\dagger} \mathbf{a}(\varphi_{l^\dagger}, N_S) \mathbf{a}^H(\varphi_{l^\dagger}, N_I)$.

Given \mathbf{W} , the problem of (17) can be formulated as a subproblem of θ , that is,

$$\min_{\theta} \quad \frac{\rho}{Q_c} I(\theta) + \frac{1-\rho}{Q_s} (-S^\dagger(\theta)) \quad (22a)$$

$$s.t. \quad |\theta_n| = 1, \quad \forall n = 1, \dots, N_I. \quad (22b)$$

Due to the unit-modulus constraint, the problem (22) is non-convex. The manifold optimization algorithm can effectively address the constraint (22b) by introducing a complex circle manifold $\mathcal{M}_{cc} = \{\theta \mid |\theta_n| = 1\}$, which defines the feasible region of (22). To obtain *Riemannian gradient* corresponding to the steepest ascent direction of the objective function [12], the Euclidean gradient of (22a) is first calculated, that is,

$$\nabla f(\theta) = \frac{2\rho}{Q_c} \left((\mathbf{B}_2 \odot \mathbf{C}_1^T) \theta + \tilde{\mathbf{a}}^* - \mathbf{d}_2 \right) - \frac{2(1-\rho)}{Q_s} \left((\mathbf{B}_3 \odot \mathbf{C}_1^T) \theta + \mathbf{c}_2^* \right). \quad (23)$$

By projecting $\nabla f(\theta)$ onto the corresponding tangent space, we can obtain the Riemannian gradient of (22a) as follows,

$$\text{grad } f(\theta) = \nabla f(\theta) - \text{Re} \{ \nabla f(\theta) \odot \theta^* \} \odot \theta. \quad (24)$$

The RSD algorithm is utilized to update θ iteratively. The descent direction at the i -th iteration is $\tau^{(i)} = -\text{grad } f(\theta^{(i)})$. $\theta^{(i+1)}$ is updated by *retraction* $\mathcal{R}_{\theta^{(i)}}$ [23], that is,

$$\theta^{(i+1)} = \mathcal{R}_{\theta^{(i)}}(\xi^{(i)} \tau^{(i)}) = \left[\frac{(\theta^{(i)} + \xi^{(i)} \tau^{(i)})_n}{\|(\theta^{(i)} + \xi^{(i)} \tau^{(i)})_n\|} \right], \quad (25)$$

where the stepsize $\xi^{(i)}$ can be computed by Armijo rule [53].

3.4. Overall Algorithm and Computational Complexity

The optimal \mathbf{W} and Θ are obtained via alternating optimization by using SDP and RSD, respectively. The primary complexity of solving (19) to obtain \mathbf{W} arises from handling the SDP constraint (19d), with the worst-case complexity being of the order $\mathcal{O}\left((2N_t + K)^{6.5}\right)$ [54]. In (22), finding the worst-case P_l has the complexity of order $\mathcal{O}(L)$. In the manifold-based algorithm, the dominant complexity originates from computing the Euclidean gradient (23), and updating Θ in each iteration has a complexity of $\mathcal{O}(N_t N_I^2)$ [12]. Therefore, the total computational complexity of the optimization problem (17) is approximately of order $\mathcal{O}\left(N_{iter,o} \left((2N_t + K)^{6.5} + N_{iter,i} N_t N_I^2 + L \right)\right)$, where $N_{iter,o}$ and $N_{iter,i}$ denote the number of outer iterations and inner iterations in RSD, respectively.

4. Antenna Selection-based Beamforming Design

In the previous section, the integrated signal design with a linear combination precoder ensures sufficient beampatterns towards multiple target subareas, overcoming the rank deficiency of radar waveforms [5]. However, by observing (4), we notice that the communication users are interfered by the radar probing signals. To completely remove interference from radar probing signals to communication users, we exclude radar probing signals $W_r S_r$ from composite signals $X = W_c S_c + W_r S_r$. As a result, the transmitting signal is comprised solely of dual-functional communication signals, i.e., $W_c S_c$, with $W_c \in \mathbb{C}^{N_t \times K}$ being the beamforming matrix designed for both the communication and sensing functionalities. It further incorporates antenna selection to reduce the energy consumption of the RF chain while maintaining sufficient beam patterns toward multiple targets. Further details are provided below.

4.1. Antenna Selection and DoF for radar sensing

To enhance the accuracy of target detection in the ISAC system, multiple transmit antennas are used to provide additional DoF, but it could also result in high hardware costs, energy consumption, and computational complexity. Since the number of targets and users of interest is limited, redundant transmit antennas can be reduced by antenna selection.

With the beamforming \mathbf{W}_c , the transmit signal for communication information and radar sensing can be presented as

$$\tilde{\mathbf{X}} = \mathbf{W}_c \mathbf{S}_c, \quad (26)$$

with the covariance matrix $\tilde{\mathbf{R}} = \mathbf{W}_c \mathbf{W}_c^H$. Based on $\mathbf{W}_c = [\mathbf{w}_1, \dots, \mathbf{w}_K]$, it defines the vector $\bar{\mathbf{w}}_n = [\mathbf{w}_1(n), \dots, \mathbf{w}_K(n)]^T \in \mathbb{C}^{K \times 1}$, where $\mathbf{w}_k(n)$ is the n -th component of \mathbf{w}_k and $n \in \{1, \dots, N_t\}$. We use the power of active beamforming as the criterion of a discrete indicator for the n -th antenna, i.e.,

$$1 \{ \|\bar{\mathbf{w}}_n\|_2^2 \} = \|\|\bar{\mathbf{w}}_n\|_2^2\|_0 = \begin{cases} 0 & \text{if } \|\bar{\mathbf{w}}_n\|_2^2 = 0, \\ 1 & \text{otherwise.} \end{cases} \quad (27)$$

More specifically, if the n -th antenna is selected, its beamforming power $\|\bar{\mathbf{w}}_n\|_2^2$ is positive and the corresponding indicator should be 1; otherwise, the indicator should be 0. To achieve high energy efficiency for information transmission, redundant antennas can be effectively reduced by minimizing the ℓ_0 -norm of activated transmit antennas, that is, $\|\tilde{\mathbf{w}}\|_0$ with $\tilde{\mathbf{w}} = [\|\bar{\mathbf{w}}_1\|_2^2, \dots, \|\bar{\mathbf{w}}_{N_t}\|_2^2]^T \in \mathbb{R}^{N_t \times 1}$.

However, in the ISAC system, simply minimizing the number of activated transmit antennas may not be able to provide sufficient DoF for radar sensing, since the transmit beampattern entirely depends on the covariance matrix of the transmitted signals [6][15]. Therefore, we first need to determine the minimum required DoF of the transmit signal.

In order to form sufficient beampattern towards all target subareas, we need to investigate the minimum number of required transmit antennas. It can be determined by minimizing the ℓ_0 -norm of the transmit beamforming, that is,

$$\min_{\mathbf{W}_c} \|\tilde{\mathbf{w}}\|_0 \quad (28a)$$

$$s.t. \sum_{d=1}^D \left| \mathbf{d}_d^H \text{vec}(\mathbf{W}_c \mathbf{W}_c^H) \right|^2 \leq \epsilon_p, \quad (28b)$$

$$\text{tr}(\mathbf{W}_c \mathbf{W}_c^H) = P_t, \quad (28c)$$

where (28b) presents the MSE of transmit beampattern. Various algorithms can be implemented to solve the nonconvex optimization problem, such as exhaustive search [55] and simultaneous orthogonal matching pursuit (SOMP) [56]. Once the optimum $\|\tilde{\mathbf{w}}\|_0$ is achieved, the minimum required DoF for covering target area can be obtained by counting the nonzero elements of the beamforming, that is, $D_0 = \|\tilde{\mathbf{w}}\|_0^*$.

Proposition 1: Suppose that the number of users is larger than the DoF for radar sensing, that is, $K \geq D_0$. The number of selected antennas N_{AS} should be greater than D_0 to guarantee the main lobes of the transmit beampattern.

Proof: Without extra probing signal, the beamformer \mathbf{W}_c with antenna selection has

$$\text{rank}(\tilde{\mathbf{R}}) \leq \text{rank}(\mathbf{W}_c) = \min \{N_{AS}, K\}, \quad (29)$$

where N_{AS} is the number of activated transmit antennas, that is $N_{AS} = \|\tilde{\mathbf{w}}\|_0$. The works of [6][15] suggest that the covariance matrix $\tilde{\mathbf{R}}$ determines the transmit beampattern directly. To ensure that there is enough DoF for forming beampattern to cover target area, the energy-aware beamforming with antenna selection has to satisfy the following inequality, that is,

$$N_{AS} \geq D_0, \quad (30)$$

when $K \geq D_0$. It completes the proof. ■

4.2. Beamforming Design Based on Antenna Selection

Instead of joint beamforming optimization (13a)-(13d), we develop an antenna selection-based beamforming design under the assumption that the number of users is larger than the required DoF for targets sensing. Energy-aware beamforming is developed by minimizing the MUI and the number of activated antennas while guaranteeing enough DoF for radar sensing. Mathematically, the optimization problem can be presented as

$$\min_{\mathbf{W}_c, \Theta} \frac{\rho}{Q_c} \left\| \tilde{\mathbf{H}}_{bu} \mathbf{W}_c \mathbf{S}_c - \bar{\mathbf{S}}_c \right\|_F^2 + (1 - \rho) \left(\frac{\|\tilde{\mathbf{w}}\|_0}{Q_a} - \min_l \frac{P_l}{Q_s} \right) \quad (31a)$$

$$s.t. \sum_{d=1}^D \left| \mathbf{d}_d^H \text{vec}(\mathbf{W}_c \mathbf{W}_c^H) \right|^2 \leq \epsilon_p, \quad (31b)$$

$$\|\tilde{\mathbf{w}}\|_0 \geq D_0, \quad (31c)$$

$$\text{tr}(\mathbf{W}_c \mathbf{W}_c^H) = P_t, \quad (31d)$$

$$|\theta_n| = 1, \quad \forall n = 1, \dots, N_I, \quad (31e)$$

where Q_c , Q_a and Q_s are determined empirically to balance multiple objective functions. The second term of (31a) reduces redundant transmit antennas by minimizing $\|\tilde{\mathbf{w}}\|_0$. According to *Proposition 1*, constraint (31c) ensures the necessary DoF for designing the beampattern to cover the sub-areas of targets effectively. Note that the energy-aware beamforming design only includes the transmit beamforming matrix \mathbf{W}_c . Therefore, only the MUI induced by multiple users is considered.

Remark 2: When the DoF required for radar sensing is sufficient for the given number of communication users or transmit antennas, the joint linear design of communication and radar precoders may increase the complexity of the

system and induce additional user interference. It motivates us to develop the energy-aware beamforming of (31a)-(31e). With the help of (31a) and (31c), redundant transmit antennas for sensing and communication can be effectively reduced, while the DoF for the radar beampattern design is guaranteed. Moreover, without the radar probing signal precoder, there is no radar interference to the users.

4.3. Alternating Optimization

Due to the highly coupled variables \mathbf{W}_c and Θ , the underlying optimization problem (31a)-(31e) is nonconvex. The alternating algorithm is introduced to optimize \mathbf{W}_c and Θ .

4.3.1. Optimization of \mathbf{W}_c with Given Θ

Given Θ , the subproblem w.r.t to \mathbf{W}_c is a mixed integer problem because of ℓ_0 norm. To tackle this challenge, we implemented the reweighted ℓ_1 norm to provide the closest convex approximation to the ℓ_0 norm [57]. As a result, $\|\tilde{\mathbf{w}}\|_0$ in second term of the objective function (31a) can be approximated as

$$\|\tilde{\mathbf{w}}\|_0 = \left\| \left[\|\bar{\mathbf{w}}_1\|_2^2, \dots, \|\bar{\mathbf{w}}_{N_t}\|_2^2 \right]^T \right\|_0 \approx \sum_{n=1}^{N_t} \beta_n \|\bar{\mathbf{w}}_n\|_2^2, \quad (32)$$

where the weight β_n associated with the n -th antenna is updated iteratively, that is,

$$\beta_n = \frac{1}{\|\bar{\mathbf{w}}_n\|_2^2 + \varsigma}, \quad \forall n = 1, \dots, N_t. \quad (33)$$

The non-negative regularization factor ς is a relatively small constant, i.e., $\varsigma > 0$, and $\|\bar{\mathbf{w}}_n\|_2^2$ is obtained from the last iteration.

Furthermore, the constraint (31c) that guarantees the minimum required DoF for radar sensing is nonconvex due to the ℓ_0 -norm. We approximate it as a concave form [58], such as

$$\|\tilde{\mathbf{w}}\|_0 = \sum_{n=1}^{N_t} [1 - \delta(\|\bar{\mathbf{w}}_n\|_2^2)] \approx \sum_{n=1}^{N_t} \left(1 - e^{-\|\bar{\mathbf{w}}_n\|_2^2/\xi}\right), \quad (34)$$

where ξ is a parameter to control the fitting to the ℓ_0 norm. As a result, the constraint (31c) can be recast as

$$\sum_{n=1}^{N_t} (1 - e^{-\|\bar{\mathbf{w}}_n\|_2^2/\xi}) \geq D_0. \quad (35)$$

Furthermore, $\tilde{\mathbf{R}} = \mathbf{W}_c \mathbf{W}_c^H$ yields $\|\bar{\mathbf{w}}_n\|_2^2 = \tilde{R}_{n,n}$, $\forall n = 1, \dots, N_t$, so the (32), (33) and (35) can be reformulated, and the subproblem of (31) can also be transformed by introducing an auxiliary variable t and utilizing SDP and Schur

complement, that is,

$$\min_{\mathbf{W}_c, \tilde{\mathbf{R}}, t} \frac{\rho}{Q_c} I(\mathbf{W}_c, \tilde{\mathbf{R}}) + (1 - \rho) \left(\frac{1}{Q_a} \sum_{n=1}^{N_t} \beta_n \tilde{R}_{n,n} - \frac{t}{Q_s} \right) \quad (36a)$$

$$s.t. \sum_{d=1}^D \left| \mathbf{d}_d^H \text{vec}(\tilde{\mathbf{R}}) \right|^2 \leq \varepsilon_p \quad (36b)$$

$$\sum_{n=1}^{N_t} (1 - e^{-\tilde{R}_{n,n}/\xi}) \geq D_0, \quad (36c)$$

$$\text{tr} \left((\mathbf{G}_{d,l} + \mathbf{G}_{r,l}) \tilde{\mathbf{R}} (\mathbf{G}_{d,l} + \mathbf{G}_{r,l})^H \right) \geq t, \forall l, \quad (36d)$$

$$\text{tr}(\tilde{\mathbf{R}}) = P_t, \quad \begin{bmatrix} \tilde{\mathbf{R}} & \mathbf{W}_c \\ \mathbf{W}_c^H & \mathbf{I} \end{bmatrix} \geq 0, \quad (36e)$$

where $I(\mathbf{W}_c, \tilde{\mathbf{R}}) = \text{tr}(\tilde{\mathbf{R}}\mathbf{B}_1) - 2\text{Re}(\text{tr}(P_t \tilde{\mathbf{H}}_{bu} \mathbf{W}_c))$. It is convex and can be solved by a standard convex toolbox.

4.3.2. Optimization of Θ with Given \mathbf{W}_c

Given \mathbf{W}_c , the problem (31a)-(31e) with respect to Θ is reformulated in a similar manner as (22a)-(22b), that is,

$$\min_{\theta} \frac{\rho}{Q_c} \tilde{I}(\theta) + \frac{(1 - \rho)}{Q_s} (-\tilde{\mathcal{S}}^\dagger(\theta)) \quad (37a)$$

$$s.t. \quad |\theta_n| = 1, \quad \forall n = 1, \dots, N_I, \quad (37b)$$

where $\tilde{I}(\theta) = \theta^H (\mathbf{B}_2 \odot \tilde{\mathbf{C}}_1^T) \theta + 2\text{Re}(\hat{\mathbf{a}}^T \theta - \theta^H \tilde{\mathbf{d}}_2)$ and $\tilde{\mathcal{S}}^\dagger(\theta) = \theta^H (\mathbf{B}_3 \odot \tilde{\mathbf{C}}_1^T) \theta + \tilde{\mathbf{c}}_2^T \theta + \theta^H \tilde{\mathbf{c}}_2^*$ with definitions of $\tilde{\mathbf{C}}_1 = \mathbf{H}_{br} \mathbf{W}_c \mathbf{W}_c^H \mathbf{H}_{br}^H$, $\hat{\mathbf{a}} = \text{diag}(\mathbf{H}_{br} \mathbf{W}_c \mathbf{W}_c^H \mathbf{H}_{bu}^H \mathbf{H}_{ru})$, $\tilde{\mathbf{d}}_2 = P_t \text{diag}(\mathbf{H}_{ru}^H \mathbf{W}_c^H \mathbf{H}_{br}^H)$, and $\tilde{\mathbf{c}}_2 = \text{diag}(\mathbf{H}_{br} \mathbf{W}_c \mathbf{W}_c^H \mathbf{G}_{d,l}^H \mathbf{G}_{rts,l}^\dagger)$.

Similarly to (22a)-(22b), this subproblem can also be solved by RSD in the complex circle manifold. The Euclidean gradient of (37a), the corresponding Riemannian gradient and the update of θ at the $(i + 1)$ -th iteration can obtained respectively

$$\nabla \tilde{f}(\theta) = \frac{2\rho}{Q_c} \left((\mathbf{B}_2 \odot \tilde{\mathbf{C}}_1^T) \theta + \hat{\mathbf{a}}^* - \tilde{\mathbf{d}}_2 \right) - \frac{2(1 - \rho)}{Q_s} \left((\mathbf{B}_3 \odot \tilde{\mathbf{C}}_1^T) \theta + \tilde{\mathbf{c}}_2^* \right), \quad (38)$$

$$\text{grad } \tilde{f}(\theta) = \nabla \tilde{f}(\theta) - \text{Re} \left\{ \nabla \tilde{f}(\theta) \odot \theta^* \right\} \odot \theta, \quad (39)$$

$$\theta^{(i+1)} = \mathcal{R}_{\theta^{(i)}} \left(-\xi^{(i)} \text{grad } \tilde{f}(\theta^{(i)}) \right). \quad (40)$$

Based on (40), the phase shift θ is successively updated until the objective value of (37a) converges.

4.4. Overall Algorithm and Computational Complexity

The optimization problem (31) is solved iteratively using SDP and RSD approaches. The complexity to solve the subproblems (36) via SDP is of order $\mathcal{O}\left((N_t + K)^{6.5}\right)$. The complexity of finding the worst-case P_l is of order $\mathcal{O}(L)$, and the complexity of updating Θ by solving (37) is of order $\mathcal{O}(N_t N_I^2)$. Consequently, the total computational complexity of the problem (31) is roughly of the order $\mathcal{O}\left(N_{iter,o}\left((N_t + K)^{6.5} + N_{iter,i}N_t N_I^2 + L\right)\right)$.

5. Simulation Results

In this section, we investigate the performance of the proposed beamforming designs on the RIS-aided ISAC system operating under sub-6GHz. The simulation layout is shown in Fig.2. The BS equipped with $N_t = 10$ transmit antennas communicates $K = 4$ users and tracks $T = 3$ potential targets. The RIS equipped with $N_I = 16$ reflecting elements and $N_s = 8$ sensors, are 105 m from the BS at an azimuth angle of 24° . Users are randomly located within the azimuthal angle of $[-4^\circ, 20^\circ]$ and at distances ranging from 100 m to 140 m from the BS. The target area is located at a distance of [90 m, 130 m] from the BS, which is divided into three subareas with corresponding angles ranging from -22° to -14° , -4° to 4° , and 14° to 22° respectively, with a grid spacing of 1° . Specifically, d_1 , d_2 , and d_3 represent the distances of subarea-1, subarea-2, and subarea-3 from the BS, respectively. The distance-dependent path loss for user-related links is modelled as $PL = PL_0 - 10\alpha \log_{10}\left(\frac{\bar{d}}{d_0}\right)$, where $PL_0 = -30$ dB, $d_0 = 1$ m, and \bar{d} represents the distance of the link [59]. The path loss exponents for channels \mathbf{H}_{bu} , \mathbf{H}_{br} and \mathbf{H}_{ru} are set as $\alpha_{bu} = 3.5$, $\alpha_{br} = 2.5$ and $\alpha_{ru} = 2.2$, respectively. We adopt the complex path loss $\rho_{ld} = \sqrt{\frac{v^2 \kappa}{64\pi^3 d_{bl}^2 d_{lr}^2}}$ for the direct link \mathbf{G}_d and $\rho_{lr} = \sqrt{\frac{v^2}{16\pi^2 d_{br}^2}} e^{j\frac{2\pi d_{br}}{v}} \sqrt{\frac{v^2 \kappa}{64\pi^3 d_{lr}^4}}$ for the RIS-reflected link \mathbf{G}_r [26], where the radar cross section (RCS) $\kappa = 7$ dBsm¹, the wavelength $v = 0.2$ m, and d_{bl} , d_{lr} , d_{br} denote the distance from the BS to the potential target t , the possible target t to the sensors at RIS, and the BS to RIS, respectively. The reflectivity of the possible target t β_t is set as 1. The noise powers at the users and the sensors are $\sigma^2 = \sigma_s^2 = -117$ dBm. The positive constants Q_c , Q_s and Q_a are set as 10^{-8} , 10^{-7} and 300, respectively. These parameters may be adjusted according to the changes of system parameters. The weighting factor $\rho = 0.2$, and the rest of the coefficients are set as $\varepsilon_p = 0.5$, $\zeta = 10^{-8}$, $\xi = 10^{-9}$.

The following proposed algorithms are considered.

- *JBF-PBF*: The joint transmit beamforming and passive beamforming design is proposed in (13), where $\mathbf{W} = [\mathbf{W}_c, \mathbf{W}_r] \in \mathbb{C}^{N_t \times (K + N_I)}$.
- *AS-BF*: The antenna selection-based beamforming design is proposed with the constraint (31c) on the DoF requirement, where $\mathbf{W} = \mathbf{W}_c \in \mathbb{C}^{N_t \times K}$.

For comparison, the following designs are considered.

¹The unit dBsm (per square meter) is used to measure the reflectivity of an object for radar signals, i.e., RCS, in a logarithmic scale.

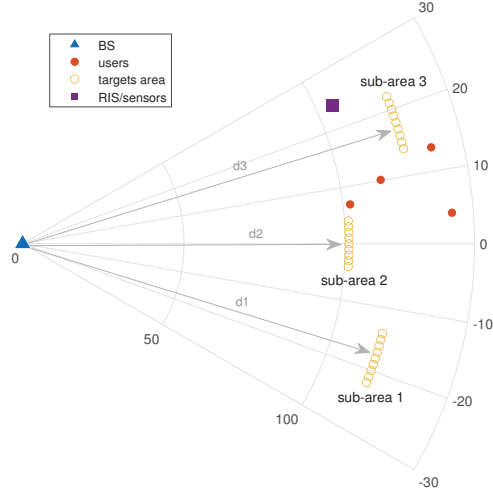


Figure 2: The top-view layout of a system setup in polar coordinates.

- *AS-BF-w/oD₀*: The antenna selection-based beamforming design is considered without the DoF constraint (31c).
- *AS-BF-w/oSNR*: The antenna selection-based beamforming design is considered without maximizing the SNR, represented by the absence of the third term in objective function (31a).
- *AS-BF-RanTheta*: The antenna selection-based beamforming design is implemented without optimizing RIS phase shift matrix, that is, the phase shift matrix is randomly generated.
- *MUI-Only*: This benchmark minimizes the MUI of users under the total transmit power constraint in the communication-only system [60]. The *MUI-Only* scheme provides an upper bound of communication performance without considering sensing metrics.
- *SNR-Only*: This benchmark maximizes the worst-case SNR at sensors adjacent to RIS elements, subject to the constraint of the total transmit power in the bistatic radar system. It provides an upper limit of the sensing performance in the radar-only system [26].

5.1. Convergence and DoF Investigation for Beampattern

Fig. 3 shows the convergence behaviour of the proposed algorithms under two power budgets, that is, $P_t = 0.5$ W and $P_t = 0.8$ W. As expected, the *JBF-PBF* design can converge after 3 or 4 iterations. The *AS-BF* and *AS-BF-w/oD₀* schemes require more iterations due to the antenna selection process. Moreover, high transmit power would lead to high converged values. Regardless of the number of communication users, the *JBF-PBF* design can achieve the lowest convergent value due to the rank-sufficient covariance matrix of the transmit signal. The *AS-BF-w/oD₀* with the least number of activated transmit antennas achieves smaller MUI than the *AS-BF* design.

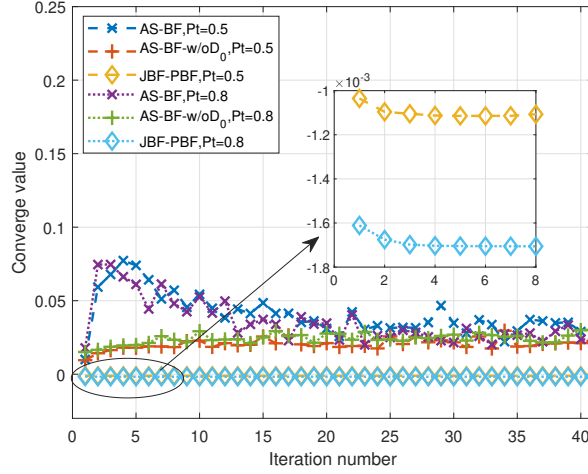


Figure 3: Convergence performance of the algorithms.

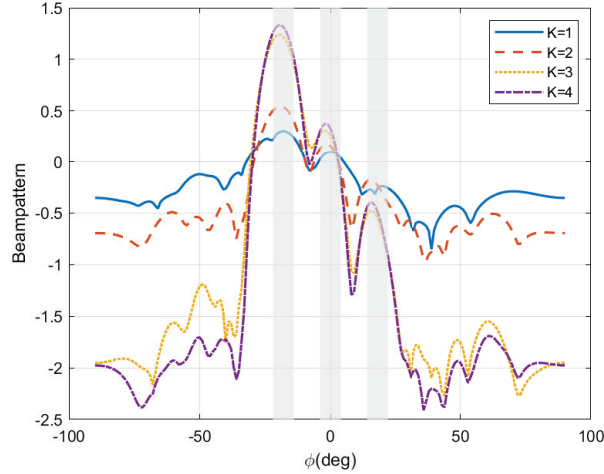


Figure 4: Transmit beampattern of *AS-BF* versus number of users ($P_t = 0.1 W$).

Fig. 4 illustrates the effect of the number of users on the transmit beampattern of the *AS-BF* design. It shows the transmit beampattern with high-amplitude main lobes and the low-amplitude sidelobe when $K = 3$ or 4. Proposition 1 suggests that when K is greater than or equal to D_0 , i.e. $K = 3$ and 4, sufficient DoF of the signal can be guaranteed for target estimation, and sufficient multiple beams can be formed towards the targets and users. Furthermore, the transmission beampattern with $K = 4$ has a slightly narrower beam than that with $K = 3$, indicating that increasing the number of users can effectively enhance the DoF of the transmission signal, which is desirable for radar sensing applications.

5.2. Effect of Transmit Covariance Matrix's DoF on Radar Performance at the Transmitter

Fig. 5 investigates the transmit beampattern under different values of maximum transmit power. The *JBF-PBF* scheme exhibits superior performance, and its enhanced sensing capabilities can be achieved by extending the DoF

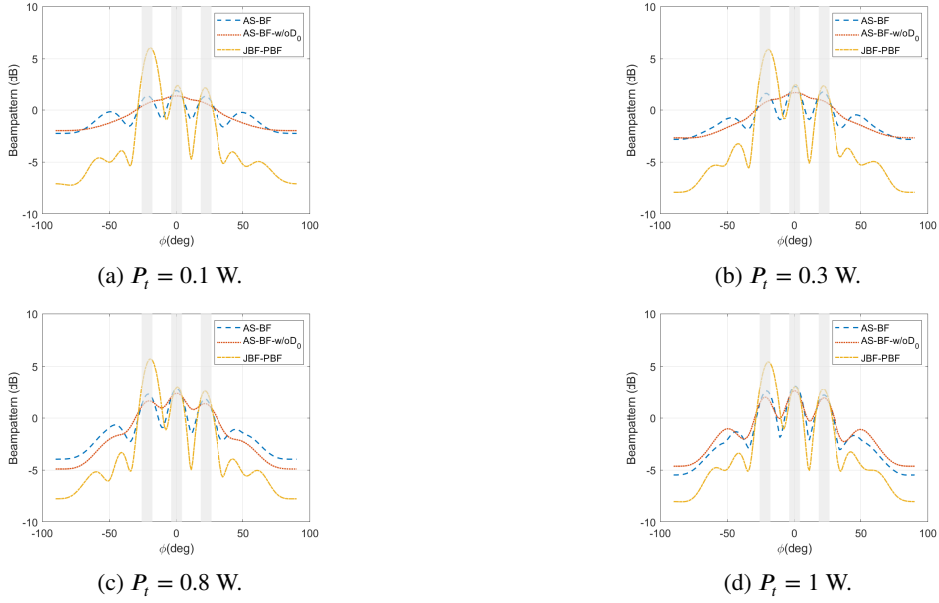


Figure 5: Transmit beampattern under different power.

of the integrated signal with an additional dimension of \mathbf{W}_r . Although the beamformer \mathbf{W}_r is not incorporated into the *AS-BF* scheme, the lower-dimensional beamforming matrix \mathbf{W}_c is designed using the antenna selection technique. As a result, the beampattern of *AS-BF* experiences a slight degradation compared to the *JBF-PBF* design. Moreover, the difference in beampattern between *AS-BF* and *JBF-PBF* becomes small as the transmit power increases. The *AS-BF-w/oD₀* scheme exhibits inferior beampattern performance due to insufficient DoF for radar sensing. To ensure a minimum DoF of radar sensing, it is recommended to adopt an antenna selection strategy to guarantee the desired beampattern. Furthermore, it can be observed that the first main lobe corresponding to the target within subarea-1, which is the furthest from the sensors, has a higher amplitude than the other target subareas. It suggests that the proposed designs would allocate high power to compensate for the severe path loss due to the long distance between the target and the sensor.

5.3. Effectiveness of Antenna Selection on Power Consumption

Fig. 6 illustrates the average achievable sum rate and the number of selected antennas versus transmit power, where the achievable sum rate of users is defined as $R = \sum_{k=1}^K \log_2(1 + \gamma_k)$. In this work, we maintain constant transmission signal power, and consequently, minimizing total interference is equivalent to maximizing the achievable sum rate of users. It is reasonable that the *MUI-Only* and *JBF-PBF* designs achieve a higher sum rate compared to the remaining designs, as they utilize all the transmit antennas. Additionally, the *JBF-PBF* design exhibits comparable performance to the *MUI-Only*, which suggests that the proposed design can effectively eliminate interference. Furthermore, the

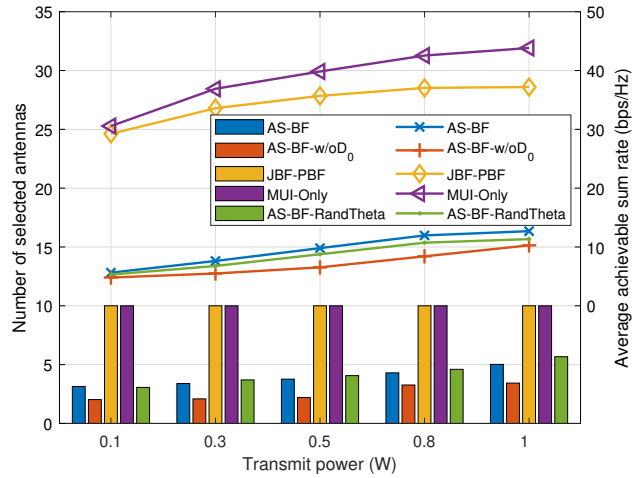


Figure 6: Average achievable sum rate and number of selected antennas versus transmit power.

AS-BF design can achieve superior performance with a reduced number of selected antennas compared to *AS-BF-RanTheta* design. It highlights the superiority of utilizing antenna selection and the deployment of RIS with the optimal phase shifts. When the transmit power increases, more antennas are activated, as the proposed antenna selection-based designs prefer to distribute the power across all antennas. Furthermore, the absence of a lower bound constraint (31c) in antenna selection means that the number of activated antennas in the *AS-BF-w/oD₀* design is less than the other designs. Among all mentioned designs, the *AS-BF-w/oD₀* design utilizes the fewest transmit antennas, consequently resulting in the lowest achievable sum rate. Furthermore, recalling Fig. 5 and Fig. 6, it can be seen that the *AS-BF-w/oD₀* design without constraint (31c) performs worse in the beampattern than the *AS-BF* design due to the less activated antennas.

5.4. Effect of Transmit Covariance Matrix's DoF on Sensing Performance at Sensors

Fig. 7 illustrates the worst SNR received in the sensors versus the transmit power, where the worst SNR is determined by the ratio of the worst received signal power at sensors to noise power. As a benchmark, the *SNR-Only* design provides the upper bound of the worst SNR, and the *AS-BF-w/oSNR* scheme provides a lower bound. The proposed *JBF-PBF* design exhibits only a slight degradation in SNR performance compared to the *SNR-Only* scheme, while manifesting an improvement compared to the *AS-BF-w/oSNR* scheme. Besides, the *AS-BF* and *AS-BF-w/oD₀* designs achieve higher worst SNR than the *AS-BF-w/oSNR* scheme, indicating incorporating antenna selection with the joint design of beamforming matrix and RIS phase shift matrix effectively enhance the worst SNR at sensors. Meanwhile, the *AS-BF-w/oD₀* design without constraint (36c) achieves lower worst SNR than the *AS-BF* design, as it prioritizes reducing transmit antenna redundancy for communication performance while neglecting the necessary DoF for target sensing.

Fig. 8 demonstrates the impact of the distance of subarea-1 from BS on the received SNR at sensors while $P_t=0.5W$. The target area consists of three subareas with d_1 being the distance from 100 m to 128 m and $d_2 = 101.1$ m and

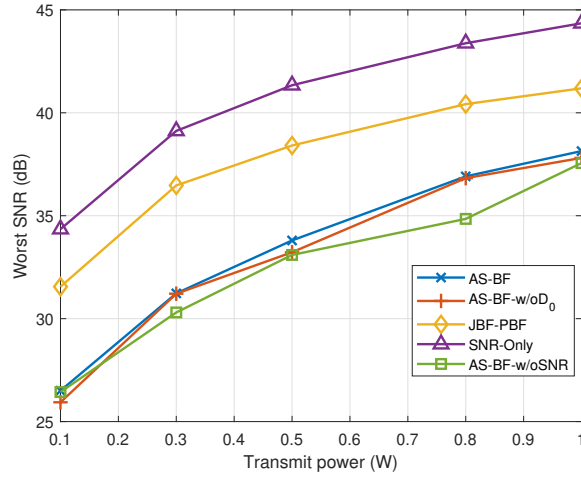


Figure 7: Worst SNR versus P_t .

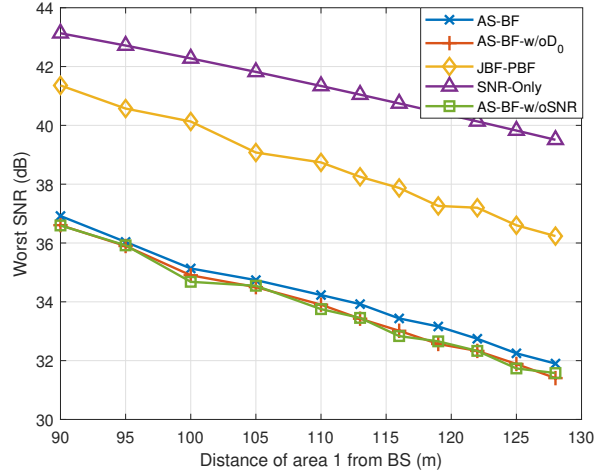


Figure 8: Worst SNR versus d_1 .

$d_3 = 121.6$ m. As the target in subarea-1 undergoes the farthest path from the BS to the sensors, d_1 is closely related to the worst case of the SNR received at the sensors. Specifically, when d_1 becomes more extensive, the received SNR performs worse. The *AS-BF* scheme exhibits superior performance to the *AS-BF-w/oSNR* design, indicating that the *AS-BF* scheme can achieve good sensing performance while reducing hardware complexity by using antenna selection to design \mathbf{W}_c .

5.5. Impact of Target Movement on Angular Separation

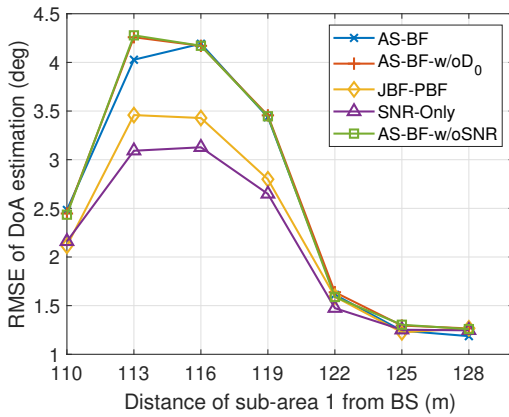
Fig. 9 further investigates the impact of the relative target locations on the sensing capabilities. Specifically, prior simulation results are predicated on the assumption that the target region are well-separated. Next, we explore the

scenario where one of the targets is moving from 110 m to 119 m, resulting in a degradation of angular separation of the target relative to the sensor. In Fig. 9(a), the root-mean-square-error (RMSE) is used as a metric to assess DoA estimation performance, where $\text{RMSE} = \sqrt{\text{E} \left\{ \frac{1}{T} \sum_{t=1}^T (\bar{\varphi}_t - \hat{\varphi}_t)^2 \right\}}$, $\bar{\varphi}_t$ is the actual angle and $\hat{\varphi}_t$ is the estimated angle for the t -th target. The DoAs of targets are estimated via the multiple signal classification (MUSIC) algorithm. When d_1 varies from 110 m to 119 m, the DoA difference between Target 1 and 2 increases, leading to a degradation in RMSE. As d_1 increases from 122 to 128 m, and the DoA difference between targets 1 and 2 is large enough, DoA can be well estimated by MUSIC, which is indicated by a smaller RMSE. The *SNR-Only* scheme provides the best performance in RMSE without considering the communication performance. With enough DoF of transmit integrated signal for sensing, *JBF-PBF* design can provide lower RMSE without considering reducing the number of activated antennas.

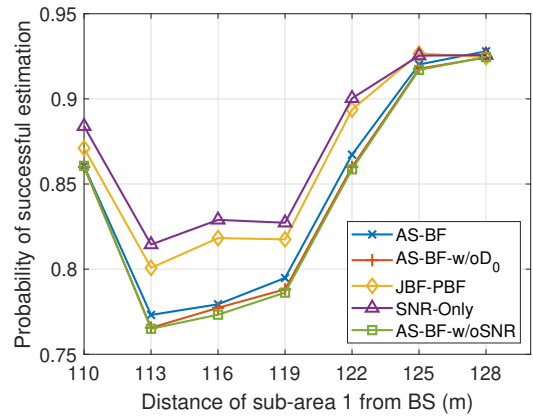
Fig. 9(b) illustrates the probability of successful DoA estimation, where d_1 varies from 110 m to 128 m. DoA estimations are considered successful if $|\bar{\varphi}_t - \hat{\varphi}_t| \leq \delta_e$ with a tunable constant δ_e , such as $\delta_e = 0.01^\circ$ [61]. The proposed algorithms are observed to exhibit better performance compared to the *AS-BF-w/oD₀* and *AS-BF-w/oSNR* designs. It is because the available DoF of the transmit signal covariance matrix for sensing targets is higher than that of the *AS-BF-w/oD₀* design. It indicates that maximization of received signal power is essential for accuracy in target estimation. Furthermore, as the DoA difference between Targets 1 and 2 increases, the probability of successful estimation gradually improves across all mentioned designs within the range of d_1 . Once the radial coordinate of Target 1 exceeds 125 m, the DoA difference between Targets 1 and 2 becomes sufficiently large to achieve high accuracy and success rates using the MUSIC algorithm.

6. Conclusion

In this work, we consider a RIS-assisted bistatic ISAC system, where the sensors are deployed near the RIS. To guarantee sufficient DoF for radar sensing, the joint precoding of communication symbols and radar probing signals with RIS phase shift is designed to minimize the total interference and maximize the worst received radar power at sensors. The SDP-RSD-based alternating optimization algorithm is utilized to obtain the optimum precoders and the RIS phase shift matrix. To further reduce the power consumption induced by RF chains and avoid interference from probing signals, an energy-aware beamforming design is developed where the minimum DoF for radar sensing is guaranteed by antenna selection based on the ℓ_0 norm. Numerical results illustrate the effectiveness of the proposed designs in sensing targets and reducing interference.



(a) RMSE of DoA estimation by MUSIC.



(b) Probability of successful estimation by MUSIC.

Figure 9: Sensing performance at sensors.

Acknowledgement

This work was supported by the NSF of China (No. 62271233), and the Basic Research Program of Guangzhou Municipal Science and Technology Bureau (No. 202102080413).

References

- [1] Liu, F., Cui, Y., Masouros, C., Xu, J., Han, T.X., Eldar, Y.C., Buzzi, S., 2022. Integrated sensing and communications: Toward dual-functional wireless networks for 6G and beyond. *IEEE J. Sel. Areas Commun.* 40, 1728–1767. doi:10.1109/JSAC.2022.3156632.
- [2] Yuan, X., Feng, Z., Zhang, J.A., Ni, W., Liu, R.P., Wei, Z., Xu, C., 2021. Spatio-temporal power optimization for MIMO joint communication and radio sensing systems with training overhead. *IEEE Trans. Veh. Technol.* 70, 514–528. doi:10.1109/TVT.2020.3046438.
- [3] Shi, S., He, Z., He, Q., Cheng, Z., 2022. Co-design for MU-MIMO communication and MIMO radar systems based on mutual information, in: *RadarConf22*, pp. 1–6. doi:10.1109/RadarConf2248738.2022.9764327.
- [4] Liu, R., Li, M., Liu, Q., Swindlehurst, A.L., 2021. Dual-functional radar-communication waveform design: A symbol-level precoding approach. *IEEE J. Sel. Topics Signal Process.* 15, 1316–1331. doi:10.1109/JSTSP.2021.3111438.
- [5] Liu, X., Huang, T., Shlezinger, N., Liu, Y., Zhou, J., Eldar, Y.C., 2020. Joint transmit beamforming for multiuser MIMO communications and MIMO radar. *IEEE Trans. Signal Process.* 68, 3929–3944. doi:10.1109/TSP.2020.3004739.
- [6] Stoica, P., Li, J., Xie, Y., 2007. On probing signal design for MIMO radar. *IEEE Trans. Signal Process.* 55, 4151–4161. doi:10.1109/TSP.2007.894398.
- [7] Keskin, M.F., Koivunen, V., Wymeersch, H., 2021. Limited feedforward waveform design for OFDM dual-functional radar-communications. *IEEE Trans. Signal Process.* 69, 2955–2970. doi:10.1109/TSP.2021.3076894.
- [8] Liu, F., Liu, Y.F., Li, A., Masouros, C., Eldar, Y.C., 2022a. Cramér-Rao bound optimization for joint radar-communication beamforming. *IEEE Trans. Signal Process.* 70, 240–253. doi:10.1109/TSP.2021.3135692.
- [9] Liu, B., Liu, J., Kato, N., 2022b. Optimal beamformer design for millimeter wave dual-functional radar-communication based V2X systems. *IEEE J. Sel. Areas Commun.* 40, 2980–2993. doi:10.1109/JSAC.2022.3196089.
- [10] Liu, F., Yuan, W., Masouros, C., Yuan, J., 2020. Radar-assisted predictive beamforming for vehicular links: Communication served by sensing. *IEEE Trans. Wireless Commun.* 19, 7704–7719. doi:10.1109/TWC.2020.3015735.

- [11] Ma, Z., Du, Q., Zhang, S., 2023. DPC-inspired beamforming design for integrated sensing and communications, in: VTC2023-Spring, pp. 1–5. doi:10.1109/VTC2023-Spring57618.2023.10200214.
- [12] Wang, X., Fei, Z., Huang, J., Yu, H., 2022. Joint waveform and discrete phase shift design for RIS-assisted integrated sensing and communication system under Cramer-Rao bound constraint. *IEEE Trans. Veh. Technol.* 71, 1004–1009. doi:10.1109/TVT.2021.3122889.
- [13] Johnston, J., Venturino, L., Grossi, E., Lops, M., Wang, X., 2022. MIMO OFDM dual-function radar-communication under error rate and beampattern constraints. *IEEE J. Sel. Areas Commun.* 40, 1951–1964. doi:10.1109/JSAC.2022.3156651.
- [14] Chen, L., Qin, X., Chen, Y., Zhao, N., 2023. Joint waveform and clustering design for coordinated multi-point DFRC systems. *IEEE Trans. Commun.* 71, 1323–1335. doi:10.1109/TCOMM.2023.3235984.
- [15] Liu, F., Zhou, L., Masouros, C., Li, A., Luo, W., Petropulu, A., 2018. Toward dual-functional radar-communication systems: Optimal waveform design. *IEEE Trans. Signal Process.* 66, 4264–4279. doi:10.1109/TSP.2018.2847648.
- [16] Zhang, H., 2022. Joint waveform and phase shift design for RIS-assisted integrated sensing and communication based on mutual information. *IEEE Commun. Lett.* 26, 2317–2321. doi:10.1109/LCOMM.2022.3195062.
- [17] Xu, Z., Liu, F., Petropulu, A., 2022. Cramér-Rao bound and antenna selection optimization for dual radar-communication design, in: ICASSP, pp. 5168–5172. doi:10.1109/ICASSP43922.2022.9747651.
- [18] Valiulahi, I., Masouros, C., Salem, A., Liu, F., 2022. Antenna selection for energy-efficient dual-functional radar-communication systems. *IEEE Wireless Commun. Lett.* 11, 741–745. doi:10.1109/LWC.2022.3142043.
- [19] Wang, Z., Mu, X., Liu, Y., 2023. STARS enabled integrated sensing and communications. *IEEE Trans. Wireless Commun.* , 1–1doi:10.1109/TWC.2023.3245297.
- [20] Liu, F., Masouros, C., Li, A., Sun, H., Hanzo, L., 2018. MU-MIMO communications with MIMO radar: From co-existence to joint transmission. *IEEE Trans. Wireless Commun.* 17, 2755–2770. doi:10.1109/TWC.2018.2803045.
- [21] Luo, H., Liu, R., Li, M., Liu, Q., 2023. RIS-aided integrated sensing and communication: Joint beamforming and reflection design. *IEEE Trans. Veh. Technol.* , 1–5doi:10.1109/TVT.2023.3248657.
- [22] Pan, C., Ren, H., Wang, K., Xu, W., El-kashlan, M., Nallanathan, A., Hanzo, L., 2020. Multicell MIMO communications relying on intelligent reflecting surfaces. *IEEE Trans. Wireless Commun.* 19, 5218–5233. doi:10.1109/TWC.2020.2990766.
- [23] Wang, X., Fei, Z., Zheng, Z., Guo, J., 2021. Joint waveform design and passive beamforming for RIS-assisted dual-functional radar-communication system. *IEEE Trans. Veh. Technol.* 70, 5131–5136. doi:10.1109/TVT.2021.3075497.
- [24] He, Y., Cai, Y., Mao, H., Yu, G., 2022. RIS-assisted communication radar coexistence: Joint beamforming design and analysis. *IEEE J. Sel. Areas Commun.* 40, 2131–2145. doi:10.1109/JSAC.2022.3155507.
- [25] Huang, N., Wang, T., Wu, Y., Wu, Q., Quek, T.Q.S., 2022. Integrated sensing and communication assisted mobile edge computing: An energy-efficient design via intelligent reflecting surface. *IEEE Wireless Commun. Lett.* 11, 2085–2089. doi:10.1109/LWC.2022.3193706.
- [26] Shao, X., You, C., Ma, W., Chen, X., Zhang, R., 2022. Target sensing with intelligent reflecting surface: Architecture and performance. *IEEE J. Sel. Areas Commun.* 40, 2070–2084. doi:10.1109/JSAC.2022.3155546.
- [27] Li, L., Yu, C., Li, Y., Huang, Z., Wu, Q., 2023. Joint squared-sine function and ANM-based DOA estimation with RIS. *IEEE Trans. Veh. Technol.* 72, 16856–16860. doi:10.1109/TVT.2023.3296137.
- [28] Hu, X., Liu, C., Peng, M., Zhong, C., 2023. IRS-based integrated location sensing and communication for mmwave SIMO systems. *IEEE Trans. Wireless Commun.* 22, 4132–4145.
- [29] Lyu, W., Yang, S., Xiu, Y., Li, Y., He, H., Yuen, C., Zhang, Z., 2024. CRB minimization for RIS-aided mmwave integrated sensing and communications. *IEEE Internet Things J.* 11, 18381–18393. doi:10.1109/JIOT.2024.3361939.

- [30] Hua, M., Wu, Q., Chen, W., Fei, Z., So, H.C., Yuen, C., 2024. Intelligent reflecting surface-assisted localization: Performance analysis and algorithm design. *IEEE Wireless Commun. Lett.* 13, 84–88.
- [31] Wang, X., Zhai, W., Wang, X., Amin, M.G., Cai, K., 2024. Wideband near-field integrated sensing and communication with sparse transceiver design. *IEEE J Sel Top Signal Process.* , 1–16.
- [32] Chen, Z., Chen, P., Guo, Z., Wang, X., 2022. A RIS-based passive DOA estimation method for integrated sensing and communication system. arXiv preprint arXiv:2204.11626 .
- [33] He, Z., Xu, W., Shen, H., Huang, Y., Xiao, H., 2022. Energy efficient beamforming optimization for integrated sensing and communication. *IEEE Wireless Commun. Lett.* 11, 1374–1378. doi:10.1109/LWC.2022.3169517.
- [34] Zhong, W., Yu, Z., Wu, Y., Zhou, F., Wu, Q., Al-Dhahir, N., 2023. Resource allocation for an IRS-assisted dual-functional radar and communication system: Energy efficiency maximization. *IEEE Trans. Green Commun. Netw.* 7, 469–482. doi:10.1109/TGCN.2022.3233839.
- [35] Kaushik, A., Masouros, C., Liu, F., 2021. Hardware efficient joint radar-communications with hybrid precoding and RF chain optimization, in: ICC, pp. 1–6. doi:10.1109/ICC42927.2021.9500661.
- [36] Sanayei, S., Nosratinia, A., 2004. Antenna selection in MIMO systems. *IEEE Commun. Mag.* 42, 68–73.
- [37] He, K., Vu, T.X., Hoang, D.T., Nguyen, D.N., Chatzinotas, S., Ottersten, B., 2024. Risk-aware antenna selection for multiuser massive MIMO under incomplete CSI. *IEEE Trans. Wireless Commun.* , 1–1.
- [38] Xu, Z., Liu, F., Diamantaras, K., Masouros, C., Petropulu, A., 2021. Learning to select for MIMO radar based on hybrid analog-digital beamforming, in: ICASSP, pp. 8228–8232. doi:10.1109/ICASSP39728.2021.9413904.
- [39] Xu, L., Sun, S., Zhang, Y.D., Petropulu, A., 2023. Joint antenna selection and beamforming in integrated automotive radar sensing-communications with quantized double phase shifters, in: ICASSP, pp. 1–5. doi:10.1109/ICASSP49357.2023.10097184.
- [40] Wang, X., Hassanien, A., Amin, M.G., 2018. Sparse transmit array design for dual-function radar communications by antenna selection. *Digit. Signal Process.* 83, 223–234.
- [41] Elbir, A.M., Abdallah, A., Celik, A., Eltawil, A.M., 2024. Antenna selection with beam squint compensation for integrated sensing and communications. *IEEE J. Sel. Top. Signal Process.* , 1–14.
- [42] Rinchi, O., Elzanaty, A., Alouini, M.S., 2022. Compressive near-field localization for multipath RIS-aided environments. *IEEE Commun. Lett.* 26, 1268–1272.
- [43] Johnson, D.H., Dudgeon, D.E., 1993. *Array signal processing: Concepts and techniques*. URL: <https://api.semanticscholar.org/CorpusID:61048422>.
- [44] Yang, R., Jiang, H., Qu, L., 2023. Waveform design for MIMO dual-functional radar-communication system using MUI energy minimization with PAPR and CRB constraints. *IEEE Commun. Lett.* 27, 1417–1421. doi:10.1109/LCOMM.2023.3259549.
- [45] Xu, D., Xu, Y., Zhang, X., Yu, X., Song, S., Schober, R., 2024. Interference mitigation for network-level isac: An optimization perspective. arXiv:2402.09974.
- [46] Kay, S.M., 1993. *Fundamentals of statistical signal processing: Estimation theory*. Prentice-Hall, Inc.
- [47] Godrich, H., Haimovich, A.M., Blum, R.S., 2010. Target localization accuracy gain in MIMO radar-based systems. *IEEE Trans. Inf. Theory* 56, 2783–2803. doi:10.1109/TIT.2010.2046246.
- [48] Fascista, A., Keskin, M.F., Coluccia, A., Wymeersch, H., Seco-Granados, G., 2022. RIS-aided joint localization and synchronization with a single-antenna receiver: Beamforming design and low-complexity estimation. *IEEE J. Sel. Topics Signal Process.* 16, 1141–1156. doi:10.1109/JSTSP.2022.3177925.

- [49] Sun, S., Petropulu, A.P., 2015. Waveform design for MIMO radars with matrix completion. *IEEE J. Sel. Topics Signal Process.* 9, 1400–1414. doi:10.1109/JSTSP.2015.2469641.
- [50] Li, B., Petropulu, A.P., 2017. Joint transmit designs for coexistence of MIMO wireless communications and sparse sensing radars in clutter. *IEEE Trans. Aerosp. Electron. Syst.* 53, 2846–2864. doi:10.1109/TAES.2017.2717518.
- [51] Wang, Z., Mu, X., Liu, Y., 2023. Bidirectional integrated sensing and communication: Full-duplex or half-duplex? *IEEE Trans. Wireless Commun.* , 1–1doi:10.1109/TWC.2023.3344229.
- [52] Boyd, S., Boyd, S.P., Vandenberghe, L., 2004. *Convex optimization*. Cambridge university press.
- [53] Jorge, N., Stephen, J.W., 2006. *Numerical optimization*. Springer, New York, NY, USA.
- [54] Zhao, M.M., Cai, Y., Zhang, R., 2023. Intelligent reflecting surface aided wireless information surveillance. *IEEE Trans. Wireless Commun.* 22, 1219–1234. doi:10.1109/TWC.2022.3203413.
- [55] Elad, M., 2010. *Sparse and redundant representations: From theory to applications in signal and image processing*. volume 2. Springer.
- [56] Singh, H., Chattopadhyay, A., 2023. Multi-target range and angle detection for MIMO-FMCW radar with limited antennas. *arXiv preprint arXiv:2302.14327* .
- [57] Candes, E.J., Wakin, M.B., Boyd, S.P., 2008. Enhancing sparsity by reweighted ℓ_1 minimization. *J. Fourier Anal. Appl.* 14, 877–905.
- [58] Malek-Mohammadi, M., Koochakzadeh, A., Babaie-Zadeh, M., Jansson, M., Rojas, C.R., 2016. Successive concave sparsity approximation for compressed sensing. *IEEE Trans. Signal Process.* 64, 5657–5671.
- [59] Hong, S., Pan, C., Ren, H., Wang, K., Nallanathan, A., 2020. Artificial-noise-aided secure MIMO wireless communications via intelligent reflecting surface. *IEEE Trans. Commun.* 68, 7851–7866.
- [60] Omid, Y., Shahabi, S.M., Pan, C., Deng, Y., Nallanathan, A., 2020. IRS-aided large-scale MIMO systems with passive constant envelope precoding. *arXiv preprint arXiv:2002.10965* .
- [61] Govinda Raj, A., McClellan, J.H., 2019. Single snapshot super-resolution DOA estimation for arbitrary array geometries. *IEEE Signal Process. Lett.* 26, 119–123. doi:10.1109/LSP.2018.2881927.